

Double Mode Cepheids from the Zwicky Transient Facility Survey

VISHWANGI SHAH,^{1,2,3,4} XIAODIAN CHEN,⁵ AND RICHARD DE GRIJS^{2,6}

¹*Birla Institute of Technology and Science, Pilani, Hyderabad Campus, India*

²*School of Mathematical and Physical Sciences, Macquarie University, Balaclava Road, Sydney, NSW 2109, Australia*

³*Department of Physics, McGill University, 3600 rue University, Montréal, QC H3A 2T8, Canada*

⁴*McGill Space Institute, McGill University, 3550 rue University, Montréal, QC H3A 2A7, Canada*

⁵*CAS Key Laboratory of Optical Astronomy, National Astronomical Observatories, Chinese Academy of Sciences, Beijing 100101, China*

⁶*Research Centre for Astronomy, Astrophysics and Astrophotonics, Macquarie University, Balaclava Road, Sydney, NSW 2109, Australia*

ABSTRACT

Multi-mode Cepheids pulsate simultaneously in more than one mode of oscillation. They provide an independent means to test stellar models and pulsation theories. They can also be used to derive metallicities. In recent years, the number of known multi-mode Cepheids has increased dramatically with the discovery of a large number of Galactic double-mode Cepheids. To date, 209 double-mode Cepheids have been detected in the Galactic bulge and disk, mostly based on the Optical Gravitational Lensing Experiment’s (OGLE) catalog. In this paper, we conduct a comprehensive search for double-mode Cepheids in the northern sky based on Zwicky Transient Facility Data Release 5. We found 72 such objects in the Milky Way. The periods of the 30 sample objects already included in the OGLE catalog show excellent agreement with the OGLE periods. The period ratios of our new Cepheids are consistent with those of known double-mode Cepheids, as evidenced by their loci in the so-called ‘Petersen diagram’. Compared with OGLE, the completeness of our double-mode Cepheid sample is around 71%. The much improved temporal sampling of the Zwicky Transient Facility offers significant scope to find more double-mode Cepheids, especially at the distribution’s short-period end.

Keywords: Cepheid variable stars (218); Double-mode Cepheid variable stars (402); Milky Way Galaxy (1054); Astronomy databases (83)

1. INTRODUCTION

Classical Cepheids are pulsating yellow giant or supergiant stars that exhibit periodic variations in their surface temperatures and luminosities. They are extremely bright and characterized by luminosities equivalent to $500\text{--}3 \times 10^4 L_{\odot}$ which makes them observable and distinguishable out to distances of up to ~ 30 Mpc or more (de Grijs 2017). Moreover, they exhibit a tight period–luminosity relationship, which makes them crucial contributors to the cosmic distance ladder.

Cepheids may exhibit a range of oscillation modes, including in their fundamental (F) mode, as well as in their first and/or second overtones (1O/2O). They sometimes oscillate in more than one mode at the same time, thus producing double- and even triple-mode Cepheids (Moskalik & Kołaczowski 2009). The period ratio for Cepheids pulsating in both the first- and second-overtone modes is $P_{21} = P_2/P_1 \simeq 0.80$, while for Cepheids pulsating in both the fundamental and first overtone modes, $P_{10} = P_1/P_0 \simeq 0.72$ (Soszyński et al. 2020a). The period ratios of the F/1O double-mode Cepheids in the Milky Way, the Large Magellanic Cloud (LMC), and the Small Magellanic Cloud (SMC) are different, that is, Cepheids in those galaxies occupy different regions in the so-called ‘Petersen diagram’ (Petersen 1973), as a result of their different metallicities (Buchler & Szabó 2007). The Petersen diagram covers the parameter space defined by the ratio of the shorter to the longer period versus the logarithm of the longer period (Soszyński et al. 2017, 2020b; Udalski et al. 2018).

Multi-mode Cepheids play an important role in studies of stellar evolution, since they probe the structure of the stellar envelope and can be used to test pulsation theories (Stobie & Balona 1979; Smolec & Moskalik 2010). The period ratios of multi-mode Cepheids can be used to determine their masses and radii without the need to know their luminosities, effective temperatures, or surface gravities (Stobie 1980; Moskalik et al. 1992). On the other hand, P_{10} of multi-mode Cepheids can be used to determine their metallicities. Sziládi et al. (2007) and Kovtyukh et al. (2016) calibrated the relationship between P_1/P_0 and $[\text{Fe}/\text{H}]$ using high-resolution spectroscopy. Those authors used it to study the metallicity distributions of the young stellar populations in the Magellanic Clouds. Lemasle et al. (2018) applied this same calibration to the F/1O double-mode Cepheids discovered by *Gaia* (Clementini et al. 2019) to derive the metallicity gradient in the Galactic disk.

Extragalactic multi-mode Cepheids have been studied by many authors, e.g., in M31 (Lee et al. 2013; Poleski 2013), M33 (Beaulieu et al. 2006), the LMC (Alcock et al. 1999; Soszyński et al. 2008; Marquette et al. 2009), and the SMC (Marquette et al. 2009; Soszyński et al. 2010). Multi-mode Cepheids in the Milky Way are more valuable, but their number included only a few dozen objects prior to 2018. Since then, the Optical Gravitational Lensing Experiment’s (OGLE) catalog (Soszyński et al. 2017, 2020b; Udalski et al. 2018) now contains 1973 Cepheids located in the Milky Way’s bulge and disk. Approximately 11% (209) of these Cepheids are F/1O and 1O/2O double-mode Cepheids (Soszyński et al. 2020a). Jurcsik et al. (2018) found 15 multi-mode Cepheids based on the ASAS-SN variables catalog (Jayasinghe et al. 2018, 2020). NASA’s Transiting Exoplanet Survey Satellite (TESS) data is suitable to find multi-mode Cepheids with smaller amplitudes (Plachy et al. 2021). Chen et al. (2020) found about 700 new Cepheids based on Zwicky Transient Facility (ZTF) Data Release 2 (DR2). *Gaia* has also been used to detect new Cepheids (Ripepi et al. 2019), as have the Asteroid Terrestrial-impact Last Alert System (Heinze et al. 2018) and the Wide-field Infrared Survey Explorer (Chen et al. 2018). Combining these Cepheid catalogs, here we report on a comprehensive search for double-mode Cepheids based on ZTF DR5.¹ Section 2 describes the data and methods used in our analysis. Section 3 outlines the results obtained, which we discuss in Section 4. We conclude the paper in Section 5.

2. DATA AND METHODS

ZTF is a robotic optical time-domain survey that uses the 48-inch Samuel Oschin Telescope at Palomar Observatory (Masci et al. 2019). It has a 47 deg² field of view, which enables observation of the entire visible northern sky. It provides photometry in the g and r bands. ZTF’s main science goal is the detailed study of variable and transient astrophysical sources (Graham et al. 2019). For public survey purposes, the entire sky visible from Palomar Observatory is observed every three nights, whereas the visible Galactic plane is covered every night. Over a period of three years, some 10⁹ sources have been observed 300–500 times each. ZTF DR5 contains data acquired between 2018 March and 2021 January.

Combining the Cepheid catalogs referred to in Section 1, we found 1436 classical Cepheids in the Milky Way that were well sampled in ZTF DR5. There were instances where a particular source was observed more than once and thus had different observation IDs (oids; see below). We identified the different observations corresponding to every single source and merged them. Bad observational epochs were removed from the light curves by adopting `catflags` < 32768. Some light curves contained clusters of data points with a cadence of less than 0.001 days. We also removed those data points, since they tended to skew our period analysis toward incorrect periods by weighing those short-cadence points disproportionately. Finally, we excluded Cepheids for which we had access to fewer than 20 observational epochs.

We performed period analysis of our sample sources based on Lomb–Scargle periodograms (Lomb 1976; Scargle 1982). The Lomb–Scargle periodogram is the most suitable technique to obtain periods based on unevenly spaced data. We used the python function `astropy.timeseries.LombScargle` to derive Lomb–Scargle periodograms from the Cepheids’ light curves. This function returns a power spectrum in the form of an array of frequencies and their corresponding powers. We set the minimum and maximum frequencies of the power spectrum to 0.00001 day^{−1} and 10 day^{−1}, respectively, since ZTF periods are found within this frequency range (e.g., Chen et al. 2020). We also set the samples-per-peak to 40 so as to make sure that our grid sampled each peak sufficiently well. The frequency corresponding to the highest peak in the power spectrum was recorded and its reciprocal value was adopted as the primary period (P_1). The light curves were pre-whitened with P_1 , i.e., the Fourier peak corresponding to P_1 was removed, and a second power spectrum was obtained to find any secondary periods (P_2). For most sample objects, $P_1 > P_2$, although a small number of objects resulted in $P_2 > P_1$. We recorded such cases as well.

¹ <https://www.ztf.caltech.edu/page/dr5>

The uncertainties in our periods were expressed using their ‘false alarm probabilities’ (FAPs). The FAP is a means to quantify the significance of a periodogram peak. It quantifies the probability that a data set with no periodic signal may yield a peak of similar magnitude because of a coincidental alignment of random errors (VanderPlas 2018). We excluded all sources that had FAPs for the primary and/or secondary periods > 0.001 . We visually analyzed the phase-folded light curves of all our sources and excluded those sources that did not show clear periodic trends, those that had folded light-curve shapes similar to those of eclipsing binaries, those where P_2 was an alias (multiple) of P_1 , those that were demonstrably aliased because of the daily observational cadence, and those whose aliased frequencies (f) coincided with the equivalent combination of P_1 and P_2 , i.e., where $f \equiv f_{P_1} \pm f_{\text{aliased}} \simeq f_{P_2}$.

The FAP for the highest peak (FAP1) was recorded. We folded the light curve with P_1 and fitted it with a tenth-order Fourier function. The best-fitting function was subtracted from the light curve, returning residual magnitudes at each observational epoch. This same procedure was repeated for the residual data to obtain P_2 and the corresponding FAP2.

Valid P_2 values satisfied $0.65 < P_2/P_1 < 0.85$ if $P_2 < P_1$ (or $0.65 < P_1/P_2 < 0.85$ if $P_1 < P_2$). These limits were adopted based on the distinct loci occupied by the Milky Way’s F/1O and 1O/2O classical Cepheids in the Petersen diagram. We applied our periodogram analysis to both the g and r data, and we adopted a source as a candidate double-mode Cepheid if it satisfied our selection criteria in at least one passband. For almost all sources in our data set, the resulting periods, both P_1 and P_2 , were identical in both filters. In a small number of cases, we obtained multiple possible values for the secondary periods. This condition applied to three objects, covered by six different oids. Specifically,

1. oids 539103300012020 and 539203300061346 referred to the same object (ZTFJ185513.28+081813.6, $P_1 = 1.86719$ d) but returned 1.38460 d and 1.34256 d as the P_2 values (with $P_1 > P_2$) in the g and r bands, respectively. We chose the period 1.34256 d as the real P_2 value, because it had a significantly smaller FAP2.
2. oids 461102300023057 and 461202300006319 (ZTFJ065417.34+012748.2, $P_1 = 0.64064$ d) yielded three different P_2 values, 0.52908 d and 0.47214 d (for $P_1 > P_2$) in the g and r bands, respectively, and additionally 0.89663 d (for $P_2 > P_1$) in the r band. This Cepheid is unlikely a double-mode Cepheid, because the amplitude of the second period is lower than expected for double-mode Cepheids (~ 0.03 mag) and the period ratio is inconsistent with other double-mode Cepheids.
3. oids 461110100019729 and 461210100026719 (ZTFJ065759.85+053444.9, $P_1 = 0.97814$ d) returned three different light-curve fits. For $P_1 > P_2$, the corresponding P_2 value was 0.79866 d in the g and r bands, but for $P_2 > P_1$ the g -band value of P_2 was 1.33215 d. The P_1 value for all three cases was 0.97814 d. We found that this is a triple-mode Cepheid with a fundamental period of 1.33215 d, a first-overtone period of 0.97814 d, and a second-overtone period of 0.79866 d, since the two period ratios resulting from these choices agree well with those of other double-mode Cepheids.

Our final tally of double-mode Cepheid candidates (see Table 1) includes 72 objects. Of those, 49 sources were detected in both the g and r bands, where they yielded the same P_1 and P_2 values, 14 sources were detected only in the g band, and nine sources were detected only in the r band. Figures 1 and 2 show examples of double-mode Cepheids identified in our analysis.

We assigned modes (F/1O or 1O/2O) to the double-mode Cepheids based on their period ratios. The OGLE F/1O and 1O/2O Cepheids occupy specific loci in the Petersen diagram, such that their period ratios lie between 0.65 and 0.85 (Soszyński et al. 2020a). For the Galactic double-mode Cepheids included in the OGLE catalog (Soszyński et al. 2017, 2020b; Udalski et al. 2018), sources with period ratios > 0.769 were classified as 1O/2O and those with period ratios < 0.769 were classified as F/1O double-mode Cepheids. We used the same selection criteria to classify our ZTF-based sample of double-mode Cepheid candidates.

3. RESULTS

For our 72 double-mode Cepheid candidates, Table 1 lists their ZTF ID, right ascension (J2000), declination (J2000), P_1 , FAP1, P_2 , FAP2, period ratio, and mode. Thirty of these Cepheids were already included in the OGLE database. Table 2 lists the OGLE periods as well as the periods resulting from our analysis of the sources in common. Our periods are in excellent agreement with the OGLE periods. Following a comparison with other double-mode Cepheid catalogs, we found that five double-mode Cepheids were detected in analyses based on the ASAS-SN database (Jurcsik

et al. 2018). Sixty-one of our candidates were identified as double-mode Cepheid candidates in a recent paper based on all available databases (Pietrukowicz et al. 2021), while 11 double-mode Cepheid candidates are newly detected.

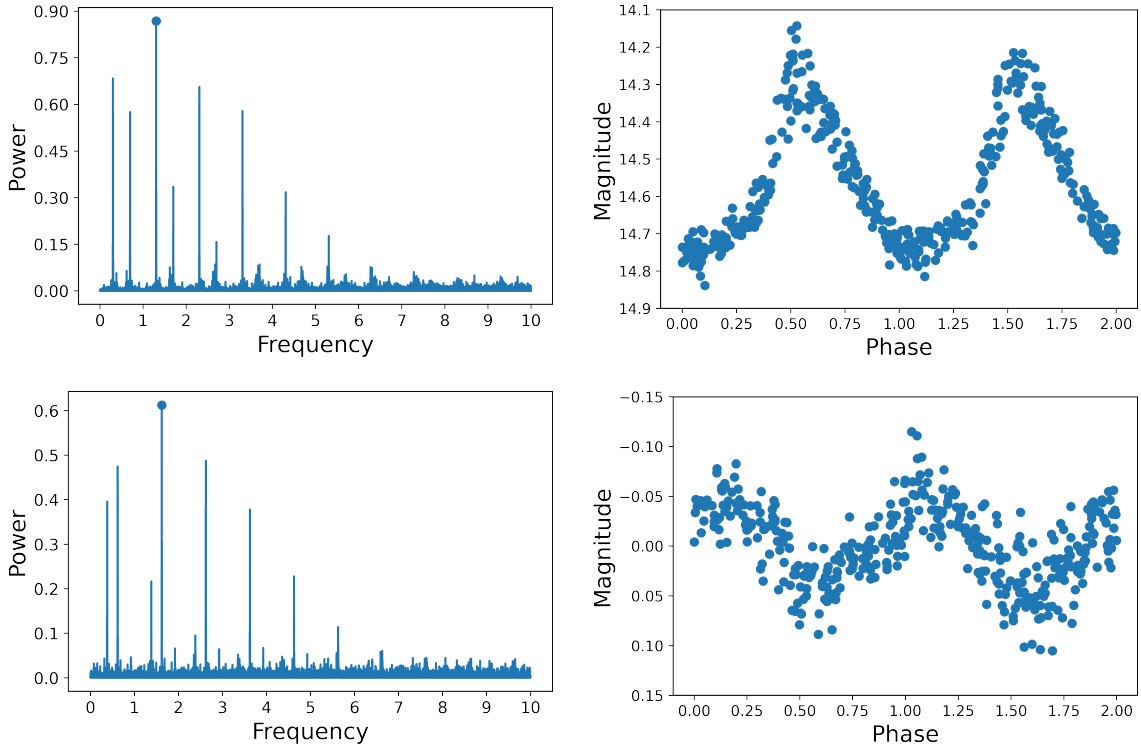


Figure 1. Power spectra and folded light curves for the double-mode Cepheid ZTFJ195955.52+363159.9. (Top left) Power spectrum of the original data with the highest peak (P_1) marked; (top right) Original light curve phased with P_1 ; (bottom left) Power spectrum after pre-whitening of the original light curve with P_1 , with the highest peak (P_2) marked; (bottom right) Pre-whitened light curve phased with P_2 after removing the power spectrum peaks corresponding to $2f_{P_2}$, $3f_{P_2}$, $(f_{P_1} + f_{P_2})$, and $(f_{P_2} - f_{P_1})$.

4. DISCUSSION

Figure 3 shows our new double-mode Cepheids (those not included in the OGLE database) in the Petersen diagram, along with the Galactic double-mode Cepheids from OGLE. P_S/P_L represents the ratio of the shorter and longer periods, whereas $\log(P_L)$ is the logarithm of the longer periods. The loci of our ZTF Cepheids are in excellent agreement with the trend followed by the OGLE Cepheids. One of our double-mode Cepheid candidates, with $P_S/P_L = 0.67876$, $P_1 = 1.17888$ days, and $P_2 = 1.73681$ days is located outside the expected F/10 locus in the Petersen diagram. This object might be a 10 Cepheid exhibiting additional low-amplitude periodicity (e.g., Ziłkowska et al. 2020). The diagram shows that all of our double-mode Cepheids are found toward the higher end of the P_L range. This is likely driven by the selection criteria adopted by Chen et al. (2020), which particularly affects the reliability of our selection of short-period Cepheids ($P_1 < 1$ day). In the absence of luminosity information, these candidate Cepheids may be contaminated by other types of short-period variables given the similarities in their light curves at these short periods and in view of the prevailing parallax uncertainties.

Table 1. Double-mode Cepheids in ZTF DR5

ZTF ID	R.A. (J2000)	Dec. (J2000)	P_1	FAP1	P_2	FAP2	Period Ratio	Modes
	(deg)	(deg)	(days)		(days)			
ZTFJ213546.72+564559.3 ^b	323.9446686	56.7664807	0.75803	3.02E−45	0.60960	1.56E−04	0.80419	1O/2O
ZTFJ035930.54+505514.2 ^c	59.8772594	50.9206351	3.37295	7.41E−90	2.44433	2.74E−04	0.72469	F/1O
ZTFJ044322.92+465704.3 ^a	70.8455148	46.9512165	0.97555	8.32E−97	0.78273	5.21E−36	0.80235	1O/2O
ZTFJ054002.90+160503.3 ^a	85.0120902	16.0842733	0.63082	4.91E−78	0.50916	2.05E−27	0.80714	1O/2O
ZTFJ055844.57+072750.2 ^b	89.6857337	7.4639545	0.68818	6.12E−47	0.55460	7.52E−12	0.80589	1O/2O
ZTFJ073008.66−194457.4 ^b	112.5361077	−19.7492858	0.69966	1.11E−47	0.56276	5.22E−10	0.80433	1O/2O
ZTFJ074310.75−113457.5 ^b	115.7948270	−11.5826560	0.71538	5.96E−32	0.57740	4.15E−14	0.80713	1O/2O
ZTFJ192918.18+220940.4 ^c	292.3257764	22.1612350	1.29991	2.88E−198	1.04274	3.67E−20	0.80216	F/1O
ZTFJ195955.52+363159.9 ^a	299.9813390	36.5333247	0.76698	8.81E−147	0.61685	2.32E−63	0.80426	1O/2O
ZTFJ200505.47+311045.0 ^a	301.2728312	31.1791667	1.88221	2.49E−98	1.50721	8.21E−18	0.80076	1O/2O
ZTFJ202946.50+374539.3 ^a	307.4437803	37.7609270	4.29728	3.48E−105	2.99001	1.24E−45	0.69579	F/1O
ZTFJ205001.31+462426.6 ^a	312.5054615	46.4073893	0.76147	9.26E−189	0.61109	1.07E−20	0.80251	1O/2O
ZTFJ205451.68+481851.5 ^b	313.7153451	48.3143193	1.64799	2.97E−76	1.18856	1.28E−45	0.72121	F/1O
ZTFJ210226.95+460422.8 ^c	315.6122978	46.0730071	0.94812	3.02E−153	0.76080	7.86E−50	0.80243	1O/2O
ZTFJ211100.38+480237.4 ^a	317.7516196	48.0437494	1.13506	1.69E−137	0.91295	6.64E−33	0.80432	1O/2O
ZTFJ222518.95+580933.8 ^a	336.3289752	58.1594015	0.99521	2.88E−160	0.80085	1.51E−14	0.80470	1O/2O
ZTFJ225650.33+622312.1 ^c	344.2097136	62.3866983	1.75898	1.16E−102	1.27310	6.04E−23	0.72377	F/1O
ZTFJ230135.57+585900.6 ^a	345.3982421	58.9835105	1.40432	4.71E−17	1.01670	5.65E−14	0.72398	F/1O
ZTFJ230636.78+621943.6 ^a	346.6532848	62.3288038	1.42788	4.78E−208	1.03493	5.69E−09	0.72480	F/1O
ZTFJ013218.14+562958.1 ^b	23.0756200	56.4994752	0.87454	2.74E−124	0.70218	4.57E−33	0.80291	1O/2O
ZTFJ015700.20+573625.9 ^a	29.2508574	57.6072142	1.04942	8.18E−128	0.84227	1.13E−66	0.8026	1O/2O
ZTFJ034219.03+542943.8 ^a	55.5793324	54.4955132	0.89610	1.09E−108	0.72071	7.87E−06	0.80428	1O/2O
ZTFJ191145.52+120006.2 ^a	287.9397036	12.0017394	1.70569	1.52E−40	1.36988	3.62E−07	0.80312	1O/2O
ZTFJ191146.64+113630.6 ^c	287.9443487	11.6085004	0.41950	7.80E−154	0.33451	7.18E−22	0.79740	1O/2O
ZTFJ190319.82+152957.6 ^a	285.8325913	15.4993410	0.25515	8.42E−126	0.20343	3.58E−17	0.79732	1O/2O
ZTFJ041005.43+614638.1 ^a	62.5226374	61.7772691	1.11338	8.54E−76	0.89471	4.05E−16	0.80360	1O/2O
ZTFJ044523.91+425520.3 ^a	71.3496452	42.9223088	0.53382	4.29E−110	0.42899	1.95E−39	0.80363	1O/2O
ZTFJ060658.08+252402.2 ^b	91.7420220	25.4006306	0.61128	6.02E−84	0.49221	5.76E−18	0.80522	1O/2O
ZTFJ183335.23−102538.0 ^b	278.3968111	−10.4272427	6.29327	2.24E−18	4.38530	9.55E−20	0.69682	F/1O
ZTFJ192801.24+195659.3 ^a	292.0051753	19.9498102	4.04453	1.30E−80	2.80727	2.80E−75	0.69409	F/1O
ZTFJ205127.87+461812.6 ^b	312.8661391	46.3035242	3.16027	2.08E−125	2.23582	5.04E−56	0.70747	F/1O
ZTFJ211839.90+504732.8 ^a	319.6662865	50.7924570	2.99769	3.80E−180	2.11915	1.60E−24	0.70693	F/1O
ZTFJ002537.70+641347.7 ^b	6.4071132	64.2299167	3.02448	6.76E−62	2.15547	9.09E−65	0.71267	F/1O
ZTFJ013859.97+645921.2 ^b	24.7499060	64.9892500	2.87147	1.64E−183	2.03188	2.93E−14	0.70761	F/1O
ZTFJ224743.67+573421.5 ^a	341.9319689	57.5726424	2.60704	2.52E−112	1.85596	9.34E−217	0.71190	F/1O
ZTFJ192549.99+194925.1 ^a	291.4583240	19.8236574	3.50719	7.69E−82	5.03600	6.56E−89	0.69643	F/1O
ZTFJ210811.91+460046.7 ^a	317.0496508	46.0129808	1.16427	7.82E−229	1.61687	3.68E−218	0.72008	F/1O
ZTFJ220413.57+574316.2 ^a	331.0565821	57.7211747	2.71994	1.38E−147	3.83044	1.12E−229	0.71009	F/1O
ZTFJ002518.14+604553.3 ^b	6.3256062	60.7648312	2.65332	1.43E−47	3.73469	1.35E−127	0.71045	F/1O
ZTFJ205714.60+462338.8 ^c	314.3108775	46.3941281	1.17888	1.31E−127	1.73681	1.74E−05	0.67876	F/1O
ZTFJ185513.28+081813.6 ^c	283.8053630	8.3037909	1.86719	8.93E−67	1.34256	3.85E−26	0.71903	F/1O
ZTFJ054703.02+174447.8 ^a	86.7625850	17.7465535	0.78963	8.54E−79	0.63560	1.36E−46	0.80493	1O/2O
ZTFJ064134.57+075639.7 ^b	100.3940561	7.9443372	1.28862	9.20E−62	1.03145	8.43E−26	0.80043	1O/2O
ZTFJ065046.49−085808.5 ^a	102.6937396	−8.9691016	2.58792	2.60E−33	3.60576	2.20E−47	0.71772	F/1O
ZTFJ071012.21−153204.2 ^a	107.5509129	−15.5345878	3.69437	1.13E−22	2.65381	1.48E−34	0.71834	F/1O
ZTFJ072219.30−154455.1 ^a	110.5805681	−15.7488266	0.82470	5.22E−42	0.66402	1.51E−26	0.80517	1O/2O
ZTFJ181640.89−105741.4 ^a	274.1703760	−10.9615102	8.52767	6.45E−64	5.91765	2.59E−58	0.69394	F/1O
ZTFJ183520.59−005344.7 ^a	278.8358106	−0.8957374	0.87136	6.40E−104	0.69966	1.96E−39	0.80295	1O/2O
ZTFJ190036.66+012230.7 ^a	285.1529969	1.3752143	4.16907	2.20E−93	2.92370	3.07E−108	0.70128	F/1O

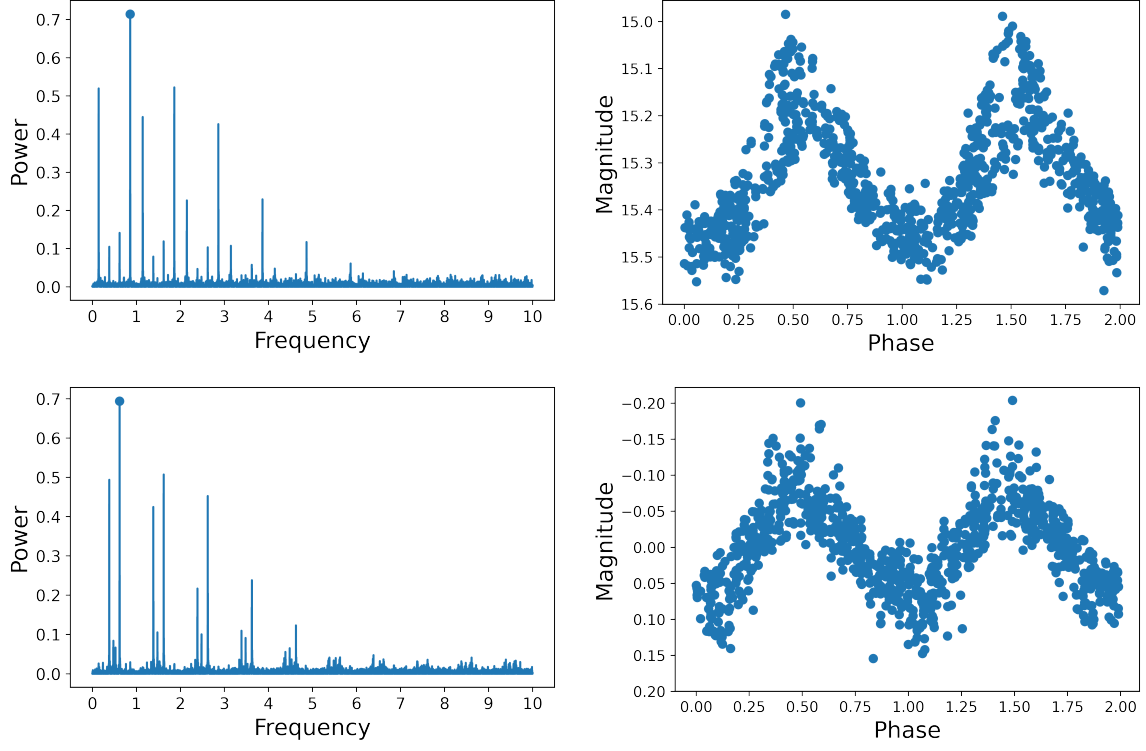


Figure 2. As Figure 1, but for the double-mode Cepheid ZTFJ210811.91+460046.7.

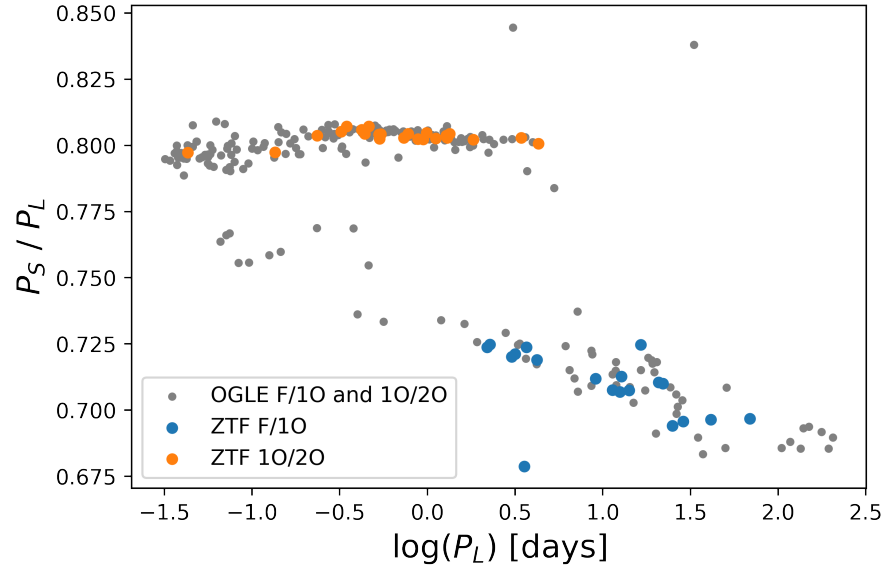


Figure 3. Petersen diagram representing the distribution of OGLE and ZTF F/10 and 10/20 Cepheids. P_S and P_L represent the shorter and longer periods, respectively. The F/10 and 10/20 Cepheids not included in the OGLE catalog are shown as blue and orange dots, respectively. The OGLE F/10 and 10/20 Cepheids are indicated by gray dots.

Among the double-mode Cepheids listed in Table 1, six have $P_1 < P_2$, including ZTFJ192549.99+194925.1, ZTFJ210811.91+460046.7, ZTFJ220413.57+574316.2, ZTFJ002518.14+604553.3, ZTFJ065046.49–085808.5, and

Table 1. (Continued.)

ZTF ID	R.A. (J2000)	Dec. (J2000)	P_1	FAP1	P_2	FAP2	Period Ratio	Modes
	(deg)	(deg)	(days)		(days)			
ZTFJ190633.59+074411.4 ^c	286.6399870	7.7365169	2.35843	1.32E−97	1.66720	3.13E−41	0.70691	F/1O
ZTFJ060249.64+184846.7 ^a	90.7069559	18.8128179	0.65314	3.38E−71	0.52635	2.47E−51	0.80588	1O/2O
ZTFJ062805.03+142806.6 ^a	97.0209950	14.4684825	0.64072	1.93E−80	0.51575	1.41E−25	0.80495	1O/2O
ZTFJ062855.82+110729.3 ^a	97.2326051	11.1248038	1.09668	2.78E−65	0.88068	1.03E−39	0.80304	1O/2O
ZTFJ071659.29−151824.8 ^b	109.2472005	−15.3070503	2.31124	9.09E−26	1.64473	8.75E−23	0.71162	F/1O
ZTFJ184059.48−054601.4 ^a	280.2478525	−5.7670548	4.80809	2.54E−53	3.28484	1.24E−27	0.68319	F/1O
ZTFJ184357.04−024614.0 ^a	280.9877159	−2.7705098	1.03738	1.43E−142	0.82907	3.22E−56	0.79920	1O/2O
ZTFJ064219.76−031854.6 ^a	100.5824297	−3.3152906	1.37668	2.02E−61	1.10499	4.52E−36	0.80265	1O/2O
ZTFJ055219.11+174439.5 ^a	88.0796577	17.7442702	0.80633	3.60E−74	0.64934	5.86E−57	0.80530	1O/2O
ZTFJ055634.35+161752.8 ^a	89.1431964	16.2979392	0.54802	5.47E−82	0.44165	7.52E−56	0.80590	1O/2O
ZTFJ062040.28+080858.7 ^a	95.1678464	8.1496330	0.93473	2.04E−110	0.75066	1.10E−79	0.80308	1O/2O
ZTFJ062542.06+082944.5 ^a	96.4252827	8.4957151	0.72783	1.61E−70	0.58714	7.76E−40	0.80670	1O/2O
ZTFJ063636.38+060931.7 ^a	99.1517198	6.1586902	0.71876	1.02E−66	0.57720	9.47E−30	0.80305	1O/2O
ZTFJ063814.13+061839.0 ^a	99.5589704	6.3107454	0.83307	3.72E−69	0.67093	4.45E−45	0.80537	1O/2O
ZTFJ063819.23+071646.5 ^a	99.5801659	7.2795846	0.49332	3.46E−75	0.39761	3.15E−15	0.80599	1O/2O
ZTFJ065015.78+033810.3 ^a	102.5657596	3.6361556	0.58819	4.67E−60	0.47334	1.91E−29	0.80474	1O/2O
ZTFJ071230.19−165412.6 ^a	108.1259255	−16.9036312	0.58938	1.47E−44	0.47620	1.38E−23	0.80797	1O/2O
ZTFJ071756.78−132534.9 ^a	109.4865826	−13.4264447	0.33334	1.04E−66	0.26785	3.69E−41	0.80353	1O/2O
ZTFJ072206.69−173810.6 ^a	110.5281129	−17.6364520	0.67705	1.57E−38	0.54572	2.70E−24	0.80603	1O/2O
ZTFJ185613.58−020059.6 ^a	284.0566073	−2.0165497	0.28563	2.12E−122	0.22656	2.29E−79	0.79319	1O/2O
ZTFJ181319.70−163319.2 ^a	273.3321638	−16.5553899	7.53182	3.97E−66	5.16720	2.52E−40	0.68605	F/1O
ZTFJ073335.45−255036.3 ^c	113.3979154	−25.8436666	2.87103	3.79E−19	2.04826	8.36E−14	0.71342	F/1O
ZTFJ222304.62+574439.5 ^a	335.7692700	57.7443300	1.12015	6.83E−172	0.89936	3.43E−95	0.80290	1O/2O

NOTE—ZTF ID: Source ID; R.A., Dec.: Source position (J2000); P_1 : Dominant period obtained from the time-series data; FAP1: Corresponding FAP; P_2 : Dominant period obtained from the light curve, pre-whitened with P_1 ; FAP2: Corresponding FAP; Period Ratio: Ratio of the shorter to the longer period; Modes: Pulsation modes of the double-mode Cepheids. ^a Sources detected in both the g and r bands and for which both P_1 and P_2 were the same in both bands; FAP values pertaining to the g band are included in the table. ^b Sources only detected in the g band; ^c Sources only detected in the r band.

ZTFJ205714.60+462338.8. For these Cepheids, the first-overtone frequencies are associated with larger amplitudes, whereas their fundamental frequencies are suppressed.

Our initial sample included 42 of OGLE’s Galactic F/1O and 1O/2O Cepheids. Of these, we identified 30 as possible double-mode Cepheids, thus suggesting that our method is 71% efficient at finding double-mode Cepheids. We analyzed the remaining 12 sources individually to determine why they were not identified by our analysis. Table 3 lists the OGLE periods of these sources, as well as the ZTF periods and FAPs returned by our analysis, and the periods and FAPs returned by running our code on the OGLE data of these sources. As is evident from the table, our analysis did not identify these candidates because the FAP values based on the ZTF data are > 0.001 . Based on the OGLE data, our code can identify these double-mode Cepheids, but their FAPs are mostly greater than 10^{-10} . This indicates that the secondary periods of these double-mode Cepheids are not significant, and the number of ZTF photometric data points is not sufficient to detect these secondary periods.

Table 2. Double-mode Cepheids returned by our analysis and already present in the OGLE catalog

OGLE ID	ZTF ID	R.A. (J2000)	Dec. (J2000)	OGLE P_1	ZTF P_1	OGLE P_2	ZTF P_2
		(deg)	(deg)	(days)	(days)	(days)	(days)
OGLE-GD-CEP-1275	ZTFJ054703.02+174447.8	86.762585	17.7465535	0.78965	0.78963	0.63559	0.63560
OGLE-GD-CEP-0057	ZTFJ064134.57+075639.7	100.3940561	7.9443372	1.28862	1.28862	1.03152	1.03145
OGLE-GD-CEP-1595 ^a	ZTFJ065046.49−085808.5	102.6937396	−8.9691016	3.60623	2.58792	2.58798	3.60576
OGLE-GD-CEP-0088	ZTFJ071012.21−153204.2	107.5509129	−15.5345878	3.69488	3.69437	2.65343	2.65381
OGLE-GD-CEP-0101	ZTFJ072219.30−154455.1	110.5805681	−15.7488266	0.82472	0.82470	0.66395	0.66402
OGLE-BLG-CEP-152	ZTFJ181640.89−105741.4	274.170376	−10.9615102	8.52790	8.52767	5.91155	5.91765
OGLE-GD-CEP-1376	ZTFJ183520.59−005344.7	278.8358106	−0.8957374	0.87137	0.87136	0.69970	0.69966
OGLE-GD-CEP-1266	ZTFJ190036.66+012230.7	285.1529969	1.3752143	4.16886	4.16907	2.92363	2.92370
OGLE-GD-CEP-1447	ZTFJ190633.59+074411.4	286.639987	7.7365169	2.35832	2.35843	1.66738	1.66720
OGLE-GD-CEP-0022	ZTFJ060249.64+184846.7	90.7069559	18.8128179	0.65317	0.65314	0.52654	0.52635
OGLE-GD-CEP-0037	ZTFJ062805.03+142806.6	97.020995	14.4684825	0.64071	0.64072	0.51575	0.51575
OGLE-GD-CEP-0039	ZTFJ062855.82+110729.3	97.2326051	11.1248038	1.09666	1.09668	0.88072	0.88068
OGLE-GD-CEP-0097	ZTFJ071659.29−151824.8	109.2472005	−15.3070503	2.31109	2.31124	1.64558	1.64473
OGLE-GD-CEP-1216	ZTFJ184059.48−054601.4	280.2478525	−5.7670548	4.80794	4.80809	3.28552	3.28484
OGLE-GD-CEP-1226	ZTFJ184357.04−024614.0	280.9877159	−2.7705098	1.03735	1.03738	0.82909	0.82907
OGLE-GD-CEP-1302	ZTFJ064219.76−031854.6	100.5824297	−3.3152906	1.37673	1.37668	1.10476	1.10499
OGLE-GD-CEP-1584	ZTFJ055219.11+174439.5	88.0796577	17.7442702	0.80632	0.80633	0.64936	0.64934
OGLE-GD-CEP-1585	ZTFJ055634.35+161752.8	89.1431964	16.2979392	0.54803	0.54802	0.44167	0.44165
OGLE-GD-CEP-1587	ZTFJ062040.28+080858.7	95.1678464	8.149633	0.93468	0.93473	0.75065	0.75066
OGLE-GD-CEP-1588	ZTFJ062542.06+082944.5	96.4252827	8.4957151	0.72781	0.72783	0.58714	0.58714
OGLE-GD-CEP-1591	ZTFJ063636.38+060931.7	99.1517198	6.1586902	0.71880	0.71876	0.57709	0.57720
OGLE-GD-CEP-1592	ZTFJ063814.13+061839.0	99.5589704	6.3107454	0.83306	0.83307	0.67106	0.67093
OGLE-GD-CEP-1593	ZTFJ063819.23+071646.5	99.5801659	7.2795846	0.49332	0.49332	0.39760	0.39761
OGLE-GD-CEP-1594	ZTFJ065015.78+033810.3	102.5657596	3.6361556	0.58812	0.58819	0.47309	0.47334
OGLE-GD-CEP-1598	ZTFJ071230.19−165412.6	108.1259255	−16.9036312	0.58939	0.58938	0.47619	0.47620
OGLE-GD-CEP-1599	ZTFJ071756.78−132534.9	109.4865826	−13.4264447	0.33334	0.33334	0.26788	0.26785
OGLE-GD-CEP-1602	ZTFJ072206.69−173810.6	110.5281129	−17.636452	0.67703	0.67705	0.54572	0.54572
OGLE-GD-CEP-1803	ZTFJ185613.58−020059.6	284.0566073	−2.0165497	0.28563	0.28563	0.22656	0.22656
OGLE-BLG-CEP-147	ZTFJ181319.70−163319.2	273.3321638	−16.5553899	7.53251	7.53182	5.16492	5.16720
OGLE-GD-CEP-0117	ZTFJ073335.45−255036.3	113.3979154	−25.8436666	2.87088	2.87103	2.04830	2.04826

NOTE—OGLE, ZTF ID: IDs in the OGLE and ZTF catalogs, respectively; R.A., Dec.: Source position (J2000); OGLE P_1 , ZTF P_1 : Dominant periods listed in the OGLE catalog and returned by our analysis of ZTF DR5 data, respectively; OGLE P_2 , ZTF P_2 : Secondary periods listed in the OGLE catalog and returned by our analysis of ZTF DR5 data, respectively.

^a Note that the ZTF P_1 and P_2 values determined for this source are equivalent to, respectively, the OGLE P_2 and P_1 values.

Table 3. OGLE double-mode Cepheids in our sample of classical Cepheids but not identified by our code

OGLE ID	ZTF ID	ZTF P_1	ZTF	OGLE P_1	OGLE	OGLE P_1	ZTF P_2	ZTF	OGLE P_2	OGLE P_2	OGLE P_2
		(days)	FAP1	(days)	FAP1	(catalog)	(days)	FAP2	(days)	FAP2	(catalog)
OGLE-GD-CEP-0064	ZTFJ064545.66-035146.5	1.83988	4.19E-92	1.83988	2.28E-107	2.54647	1.40638	9.09E-01	1.26430	9.83E-01	1.83987
OGLE-GD-CEP-0106	ZTFJ072859.96-231134.9	0.28976	1.02E-37	0.28976	3.57E-106	0.28976	0.19960	2.44E-02	0.23184	3.34E-06	0.23184
OGLE-GD-CEP-0139	ZTFJ075308.92-260300.5	0.58759	2.49E-17	0.58758	1.32E-111	0.58758	0.41502	1.56E-01	0.47246	1.42E-17	0.47247
OGLE-GD-CEP-1604	ZTFJ072512.92-210444.2	3.89821	7.07E-38	3.89919	1.84E-95	5.50298	2.95551	2.68E-01	2.97555	9.68E-01	3.89932
OGLE-GD-CEP-1612	ZTFJ074757.30-274927.5	0.23966	2.08E-32	0.23967	2.13E-95	0.23966	0.19895	3.91E-02	0.19171	6.47E-22	0.19171
OGLE-GD-CEP-1788	ZTFJ182833.76-102742.1	0.22392	2.83E-68	0.22392	6.52E-36	0.22392	0.16534	2.29E-02	0.17806	1.15E-05	0.17799
OGLE-GD-CEP-1790	ZTFJ183258.00-104302.8	0.24925	3.69E-19	0.24925	5.34E-23	0.24925	0.16409	3.75E-02	0.19817	1.69E-03	0.19817
OGLE-GD-CEP-1797	ZTFJ184711.94-090312.4	4.08245	4.07E-02	0.29994	2.91E-17	0.29994	3.07714	1.00E+00	0.24266	1.45E-03	0.24266
OGLE-GD-CEP-1798	ZTFJ184735.17-013535.0	0.61226	5.28E-54	0.61228	7.45E-49	0.61229	0.48913	1.47E-01	0.48912	5.22E-10	0.48912
OGLE-GD-CEP-1804	ZTFJ185958.20-014220.9	0.24109	2.48E-22	0.24109	2.05E-48	0.24109	0.15963	3.48E-01	0.19178	3.31E-08	0.19178
OGLE-BLG-CEP-077	ZTFJ175045.97-225949.0	0.23420	3.09E-03	3.51965	3.03E-87	3.51969	0.17751	1.00E+00	2.53351	3.20E-215	2.5330
OGLE-GD-CEP-1799	ZTFJ185322.20-085832.8	0.45989	6.81E-20	0.45987	5.53E-21	0.31474	0.34139	4.64E-31	0.34139	1.36E-29	0.25433

NOTE—OGLE, ZTF ID: IDs in the OGLE and ZTF catalogs, respectively; ZTF P_1 , P_2 : Period for the ZTF data; ZTF FAP1,FAP2: Corresponding FAP; OGLE P_1 , P_2 : Period obtained by running our code on the OGLE data; OGLE FAP1, FAP2:Corresponding FAP; OGLE P_1 , P_2 (catalog): Period listed in the OGLE catalog.

5. CONCLUSION

Our analysis of the ZTF DR5 data has identified 72 Galactic double-mode Cepheids (29 F/1O and 43 1O/2O). The loci of these Cepheids in the Petersen diagram agree with the general trend followed by double-mode Cepheids, further confirming their correct classification. Thirty double-mode Cepheids were already listed in the OGLE catalog. Our periods are in excellent agreement with the periods reported by OGLE. Twelve additional OGLE double-mode Cepheids were present in our sample but not identified by our analysis. The main reason for this is that the secondary periods of these double-mode Cepheids are of low significance and the number of ZTF photometric data points is not sufficient to detect them. Compared with OGLE, our completeness is around 71%. With better sampling of light curves in future ZTF DRs, we expect to identify an even larger number of new Galactic double-mode Cepheids, which will be complementary to the OGLE Galactic double-mode Cepheids in the northern sky.

ACKNOWLEDGEMENTS

X.C. acknowledges funding support from the National Natural Science Foundation of China (NSFC) through grants 12173047 and 11903045. This research was supported in part by the Australian Research Council Centre of Excellence for All Sky Astrophysics in 3 Dimensions (ASTRO 3D), through project number CE170100013. This publication is based on observations obtained with the Samuel Oschin 48-inch Telescope at Palomar Observatory as part of the Zwicky Transient Facility project. ZTF is supported by the U.S. National Science Foundation through grant AST-1440341 and a collaboration including Caltech, IPAC, the Weizmann Institute for Science, the Oskar Klein Center at Stockholm University, the University of Maryland, the University of Washington, Deutsches Elektronen-Synchrotron and Humboldt University, Los Alamos National Laboratories, the TANGO Consortium of Taiwan, the University of Wisconsin at Milwaukee and Lawrence Berkeley National Laboratories. Operations are conducted by Caltech Optical Observatories, IPAC and the University of Washington.

REFERENCES

- Alcock, C., Allsman, R. A., Alves, D., et al. 1999, *ApJ*, 511, 185. doi:10.1086/306638
- Beaulieu, J.-P., Buchler, J. R., Marquette, J.-B., et al. 2006, *ApJL*, 653, L101. doi:10.1086/510453
- Buchler, J. R. & Szabó, R. 2007, *ApJ*, 660, 723. doi:10.1086/513071
- Chen, X., Wang, S., Deng, L., et al. 2018, *ApJS*, 237, 28. doi:10.3847/1538-4365/aad32b
- Chen, X., Wang, S., Deng, L., et al. 2020, *ApJS*, 249, 18. doi:10.3847/1538-4365/ab9cae
- Clementini, G., Ripepi, V., Molinaro, R., et al. 2019, *A&A*, 622, A60. doi:10.1051/0004-6361/201833374
- de Grijs, R. 2011, *An Introduction to Distance Measurement in Astronomy* (Wiley), 87–90
- Graham, M. J., Kulkarni, S. R., Bellm, E. C., et al. 2019, *PASP*, 131, 078001. doi:10.1088/1538-3873/ab006c
- Heinze, A. N., Tonry, J. L., Denneau, L., et al. 2018, *AJ*, 156, 241. doi:10.3847/1538-3881/aae47f
- Jayasinghe, T., Kochanek, C. S., Stanek, K. Z., et al. 2018, *MNRAS*, 477, 3145. doi:10.1093/mnras/sty838
- Jayasinghe, T., Stanek, K. Z., Kochanek, C. S., et al. 2020, *MNRAS*, 491, 13. doi:10.1093/mnras/stz2711
- Jurcsik, J., Hajdu, G., & Catelan, M. 2018, *AcA*, 68, 341. doi:10.32023/0001-5237/68.4.2
- Kovtyukh, V., Lemasle, B., Chekhonadskikh, F., et al. 2016, *MNRAS*, 460, 2077. doi:10.1093/mnras/stw1113
- Lee, C.-H., Kodric, M., Seitz, S., et al. 2013, *ApJ*, 777, 35. doi:10.1088/0004-637X/777/1/35
- Lemasle, B., Hajdu, G., Kovtyukh, V., et al. 2018, *A&A*, 618, A160. doi:10.1051/0004-6361/201834050
- Lomb, N. R. 1976, *Ap&SS*, 39, 447. doi:10.1007/BF00648343
- Marquette, J. B., Beaulieu, J. P., Buchler, J. R., et al. 2009, *A&A*, 495, 249. doi:10.1051/0004-6361:200810842
- Masci, F. J., Laher, R. R., Rusholme, B., et al. 2019, *PASP*, 131, 018003. doi:10.1088/1538-3873/aae8ac
- Moskalik, P., Buchler, J. R., & Marom, A. 1992, *ApJ*, 385, 685. doi:10.1086/170975
- Moskalik, P. & Kołaczowski, Z. 2009, *MNRAS*, 394, 1649. doi:10.1111/j.1365-2966.2009.14428.x
- Petersen, J. O. 1973, *A&A*, 27, 89
- Pietrukowicz, P., Soszyński, I., & Udalski, A. 2021, *AcA*, 71, 205. doi:10.32023/0001-5237/71.3.2
- Plachy, E., Pál, A., Bódi, A., et al. 2021, *ApJS*, 253, 11. doi:10.3847/1538-4365/abd4e3
- Poleski, R. 2013, *ApJ*, 778, 147. doi:10.1088/0004-637X/778/2/147
- Ripepi, V., Molinaro, R., Musella, I., et al. 2019, *A&A*, 625, A14. doi:10.1051/0004-6361/201834506

- Scargle, J. D. 1982, *ApJ*, 263, 835. doi:10.1086/160554
- Smolec, R. & Moskalik, P. 2010, *A&A*, 524, A40.
doi:10.1051/0004-6361/201014494
- Soszyński, I., Poleski, R., Udalski, A., et al. 2008, *AcA*, 58, 153
- Soszyński, I., Poleski, R., Udalski, A., et al. 2010, *AcA*, 60, 17
- Soszyński, I., Udalski, A., Szymański, M. K., et al. 2017, *AcA*, 67, 297. doi:10.32023/0001-5237/67.4.1
- Soszyński, I., Udalski, A., Szymański, M. K., et al. 2020a, *AcA*, 70, 101. doi:10.32023/0001-5237/70.2.2
- Soszyński, I., Smolec, R., Udalski, A., et al. 2020b, *ApJL*, 901, L25. doi:10.3847/2041-8213/abb817
- Stobie, R. S. 1980, *SSRv*, 27, 401. doi:10.1007/BF00168326
- Stobie, R. S. & Balona, L. A. 1979, *MNRAS*, 189, 627.
doi:10.1093/mnras/189.4.627
- Sziládi, K., Vinkó, J., Poretti, E., et al. 2007, *A&A*, 473, 579. doi:10.1051/0004-6361:20077539
- Udalski, A., Soszyński, I., Pietrukowicz, P., et al. 2018, *AcA*, 68, 315. doi:10.32023/0001-5237/68.4.1
- VanderPlas, J. T. 2018, *ApJS*, 236, 16.
doi:10.3847/1538-4365/aab766
- Ziółkowska, O., Styczeń, M., & Smolec, R. 2020, XXXIX Polish Astronomical Society Meeting, 10, 75